Transport reduction by current profile control in the reversed-field pinch*

J. S. Sarff,† A. F. Almagri, M. Cekic, C.-S. Chaing, D. Craig, D. J. Den Hartog, G. Fiksel, S. A. Hokin, R. W. Harvey,[a] H. Ji, C. Litwin, S. C. Prager, D. Sinitsyn, C. R. Sovinec, J. C. Sprott, and E. Uchimoto[b]
Department of Physics, University of Wisconsin, Madison, Wisconsin 53706

(Received 21 November 1994; accepted 28 February 1995)

An auxiliary poloidal inductive electric field applied to a reversed-field pinch (RFP) plasma reduces the current density gradient, slows the growth of $m=1$ tearing fluctuations, suppresses their associated sawteeth, and doubles the energy confinement time. This experiment attacks the dominant RFP plasma loss mechanism of parallel streaming in a stochastic magnetic field. The auxiliary electric field flattens the current profile and reduces the magnetic fluctuation level. Since a toroidal flux change linking the plasma is required to generate the inductive poloidal electric field, the current drive is transient to avoid excessive perturbation of the equilibrium. To sustain and enhance the improved state, noninductive current drivers are being developed. A novel electrostatic current drive scheme uses a plasma source for electron injection, and the lower-hybrid wave is a good candidate for radio-frequency current drive. © *1995 American Institute of Physics.*

I. INTRODUCTION

In the reversed-field pinch (RFP), the loss of plasma results primarily from particle convection along stochastic magnetic field lines generated by large-amplitude magnetohydrodynamic (MHD) fluctuations. Measurements[1,2] of the magnetic-fluctuation-induced electron particle and heat losses in the Madison Symmetric Torus[3] (MST) directly identify large transport associated with the magnetic fluctuation, while in other RFP experiments,[4] the estimated magnetic-fluctuation-induced energy loss can account for the observed global energy flux. In MST, the measured fluxes agree with expectations for convective stochastic magnetic field diffusion,[5] but the electron loss occurs at the ion rate as a result of an ambipolarity constraint on the particle flux, i.e., an outward pointing electric slows the electron loss.

More than 90% of the RFP magnetic fluctuation $\tilde{B}$ results from several poloidal mode number $m=1$, toroidal mode number $n\sim 2R/a$ core-resonant tearing (or resistive kink) instabilities. The amplitudes of these fluctuations are typically $\sim 1\%$ of the mean field,[6] and the close spatial proximity of their resonant magnetic surfaces encourages magnetic island overlap and stochasticity. Since the dominant plasma loss results from this stochasticity, researchers proposed methods for reducing the fluctuation with hope of improving RFP confinement. Tearing fluctuation stems from the current density gradient, so the proposals employ auxiliary electrostatic[7] or radio-frequency (RF)[8,9] poloidal current drive in the outer region of the plasma, eliminating the need for fluctuation-dynamo sustainment of the RFP. These theoretical and computational studies demonstrate reduction of the tearing fluctuations and the restoration of closed magnetic surfaces in the core of the plasma.

In this paper the first observation of reduced transport resulting from current profile control in a RFP is presented. The experimental technique employs auxiliary inductive poloidal current drive. Unlike electrostatic or RF current drive, poloidal inductive current drive is inherently transient, since it requires a change of toroidal flux embedding the plasma, so we call the technique pulsed poloidal current drive (PPCD) to distinguish this mode of operation from the usual RFP operation. The PPCD experiment is performed in MST, a large reversed-field pinch with major radius $R=1.5$ m, minor radius $a=0.52$ m, toroidal plasma current $I_\phi \leqslant 700$ kA, and poloidal beta $\beta_\theta \sim 10\%$. The success of PPCD encourages the program of transport reduction in the RFP by current density profile control. Preparations for an electrostatic current drive experiment on MST as well as theoretical studies of lower hybrid wave current drive for RFP profile control are also discussed. These techniques might extend and enhance the improved confinement observed during PPCD.

II. INDUCTIVE POLOIDAL CURRENT DRIVE

Auxiliary to the usual inductive toroidal electric field E_ϕ, in the PPCD experiment,[10] a fast current pulse in the toroidal field coil induces a poloidal electric field E_θ to increase the poloidal current in the plasma. Figure 1 illustrates the global electrical waveforms during PPCD. The start of the pulse is marked by the vertical dashed lines in this and subsequent figures. The one-turn poloidal V_θ and toroidal V_ϕ surface voltages shown in Fig. 1(a) generate the poloidal I_θ and toroidal I_ϕ plasma currents shown in Fig. 1(b), although strong coupling prevents identifying V_θ only with I_θ, and *vice versa*. To direct E_θ for current profile flattening, the volume-average toroidal field $\langle B_\phi \rangle$ and the toroidal field at the wall $B_{\phi w}$ must decrease, as in Fig. 1(c). As intended, PPCD increases the poloidal plasma current $I_\theta = 2\pi R(B_0 - B_{\phi w})/\mu_0$ between the magnetic axis and plasma edge, which is inferred from $\oint \mathbf{B}\cdot\mathbf{dl}$ on the magnetic axis. (The axis magnetic field B_0 is estimated using a RFP equilibrium model.)[11] Note that V_θ is nonzero as I_ϕ in-

*Paper 4IA3, Bull. Am. Phys. Soc. **39**, 1607 (1994).
†Invited speaker.
[a]Permanent address: General Atomics, San Diego, California 92186.
[b]Permanent address: Department of Physics and Astronomy, University of Montana, Missoula, Montana 59812

 1070-664X/95/2(6)/2440/7/$6.00

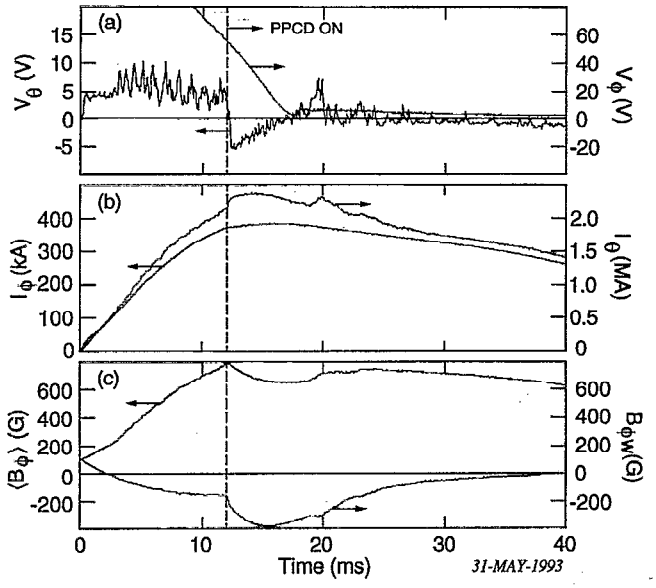

FIG. 1. Shot-averaged waveforms of (a) the surface voltages, (b) the plasma current, and (c) the average and wall toroidal field.

creases, since toroidal flux is generated by dynamo action. The Fig. 1 data are averages for 11 PPCD plasmas.

A. Current profile flattening

Since tearing instability in the RFP results from the gradient in $J_\parallel/B$, the three-parameter equilibrium model,[12]

$$\nabla\times\mathbf{B}=\lambda_0(1-r^\alpha)\mathbf{B}+(\beta_0/2B^2)\mathbf{B}\times\nabla p, \qquad (1)$$

is used to quantify the shape of the (normalized) parallel current profile $\lambda(r)=\mu_0 a\mathbf{J}\cdot\mathbf{B}/B^2$. Shape parameters α and λ_0 are adjusted to match the measured I_ϕ, $\langle B_\phi\rangle$, and $B_{\phi w}$, while the central beta value $\beta_0=2\mu_0 p_0/B_0^2$ is adjusted for assumed constant poloidal beta $\beta_\theta=2\mu_0\langle p\rangle/B_{\theta a}^2=10\%$. The pressure profile is assumed quadratic, but, in general, the perpendicular current details weakly affect the parallel current fit since β is small.

PPCD flattens the current profile in a degree comparable to a sawtooth oscillation "crash."[13] This comparison benchmarks PPCD, since in a sawtooth crash the plasma self-flattens its unstable current profile. The time evolution of α during a typical PPCD discharge is shown in Fig. 2(a). Before PPCD is applied, α varies in accordance with the sawtooth oscillation, two of which occur between 8 and 12 ms. In the sawtooth crash, α suddenly increases as the current profile flattens. When PPCD is applied at $t=12$ ms, α is increased to near the value characteristic of the profile following the crash. The PPCD phase gradually terminates as the current profile again peaks, and becomes sawtooth unstable when $\alpha\lesssim 2$. A series of unusually large sawteeth beginning at $t\approx 18$ ms cause the plasma to relax toward normal RFP equilibria.

B. Fluctuation reduction and sawtooth suppression

By flattening the current profile, PPCD slows the growth of $m=1$ fluctuations and suppresses their associated saw-

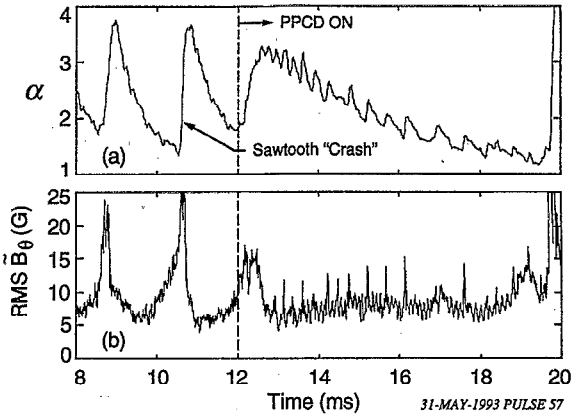

FIG. 2. (a) The current profile shape parameter $\alpha(t)$ and (b) the surface RMS poloidal magnetic field fluctuation amplitude $\tilde{B}_\theta$ during a typical PPCD discharge.

teeth. Magnetic fluctuations are measured in MST, with arrays of magnetic pickup sensors (B_θ, B_ϕ, B_r) attached to the inner vacuum vessel surface. In this work, toroidal mode $n\lesssim 15$ spectra are derived from 32 equally spaced magnetic pickup sensors. Figure 2(b) shows the spatial root-mean-square (RMS) poloidal magnetic field fluctuation amplitude $\tilde{B}_{\theta_{\rm rms}}=\sqrt{\Sigma_n \tilde{b}_{\theta n}^2}$ during the same typical discharge of Fig. 2(a). The most active modes in the spectrum $\tilde{b}_{\theta n}$ are shown in Fig. 3. Before the application of the pulse, the $(m=1)$ $n=5-10$ mode amplitudes exhibit the precursory growth associated with the sawtooth cycle. Near the times of sawtooth crash events, the amplitudes peak at about three times the value occurring between crashes. After PPCD is applied, the $n=5-10$ mode growth is dramatically slowed, and the between-crash amplitudes are maintained until $t\approx 18$ ms when sawteeth reappear. The lack of sawtoothing decreases the average fluctuation amplitude by 25% during PPCD.

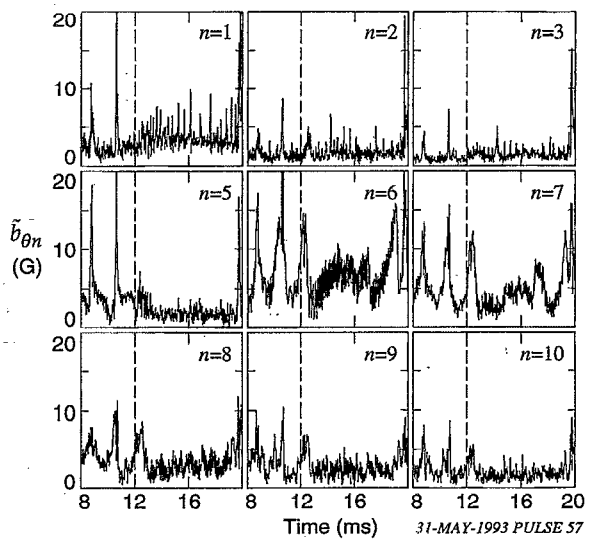

FIG. 3. Dominant modes of a single shot $\tilde{B}_\theta$ toroidal n spectrum during PPCD.

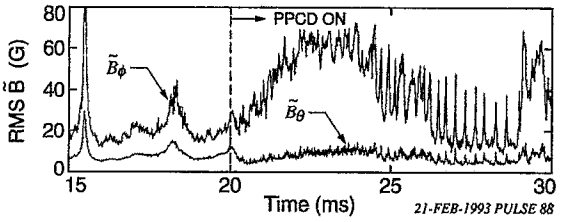

FIG. 4. The spatial RMS fluctuation amplitudes $\tilde{B}_\theta$ and $\tilde{B}_\phi$ for an overly large-amplitude PPCD pulse illustrating new $m=0$ activity.

Although PPCD suppresses sawteeth preceded by $m=1$ fluctuation, different sawtooth-like events occur during PPCD. Like conventional sawteeth, they correlate with decreases in the soft x-ray flux and increases in toroidal flux, but the amplitude changes are small. The n spectra reveal increased precursory activity in the $n=1-3$ modes, not in the band $n=5-10$. This activity, if resonant, corresponds to $m=0$ fluctuation, since the safety factor satisfies $|q(r)|\lesssim\frac{1}{5}$ during PPCD.

In addition, the low n modes grow to large amplitude when the PPCD pulse is too large (roughly when $\langle B_\phi\rangle$ is halved by the pulse). The RMS fluctuation amplitudes shown in Fig. 4 during an overly large-amplitude PPCD discharge illustrate this growth. The two-dimensional structure of the fluctuations can be inferred from these simultaneous measurements of $\tilde{B}_\phi$ and $\tilde{B}_\theta$, since the magnetic sensors are located in a current-free region, where $i\mathbf{k}\times\mathbf{B}=0$ implies $n\tilde{b}_{\theta mn}/R=m\tilde{b}_{\phi mn}/a$ for each Fourier mode $\tilde{\mathbf{b}}_{mn}$. Before PPCD is applied $\tilde{B}_\phi/\tilde{B}_\theta\approx 2$, consistent with $m=1$, $n\sim 6$ sawtooth precursors. After PPCD is applied $\tilde{B}_\phi/\tilde{B}_\theta\gtrsim 5$, consistent with $m=0, n\sim 1$ fluctuations.[14] Note that the steady growth of the $m=0$ fluctuation eventually subsides, but the new type of sawtooth-like events persist. In moderate amplitude PPCD, the steady $m=0$ growth is avoided. Interestingly, numerical modeling of the PPCD experiment using the three-dimensional (cylindrical), nonlinear, resistive MHD, initial value code DEBS[15] predicts reduced, not stabilized, $m=1$ fluctuation. However, it fails to predict enhanced $m=0$ fluctuation.

C. Transport reduction

PPCD doubles the energy confinement by halving the Ohmic input power while modestly increasing the stored thermal energy. The solid line curves in Fig. 5 show shot-averaged waveforms of (a) the central chord electron density n_e, (b) soft x-ray flux, (c) Ohmic input power P_{Ohmic} (E_θ included), and (d) H_α emission from 11 PPCD plasmas. The dashed line waveforms are for a set of eight discharges with PPCD turned off. These were produced identically to the PPCD plasmas, except a small gas puff was injected at $t=10$ ms to mimic a density increase during PPCD. The measured charge-exchange ion temperature T_i is unchanged, while the electron temperature T_e increased 25%. Here T_e is determined from shot-averaged Si(Li) detector x-ray energy spectra, taking into account impurity line radiation contributions to the x-ray spectrum. (Previous analysis indicates these diagnostics measure core temperatures.) At $t=17$ ms, $T_e\approx 250$ eV with PPCD and $T_e\approx 200$ eV without PPCD; the latter is consistent with the most recent database of MST Thomson scattering data.[16] (The single-point Thomson scattering diagnostic was inoperable during this PPCD experiment.) Other improvements include reduced total radiated power and a 20% reduction in Z_{eff} inferred from near-infrared bremmstrahlung radiation measurements.

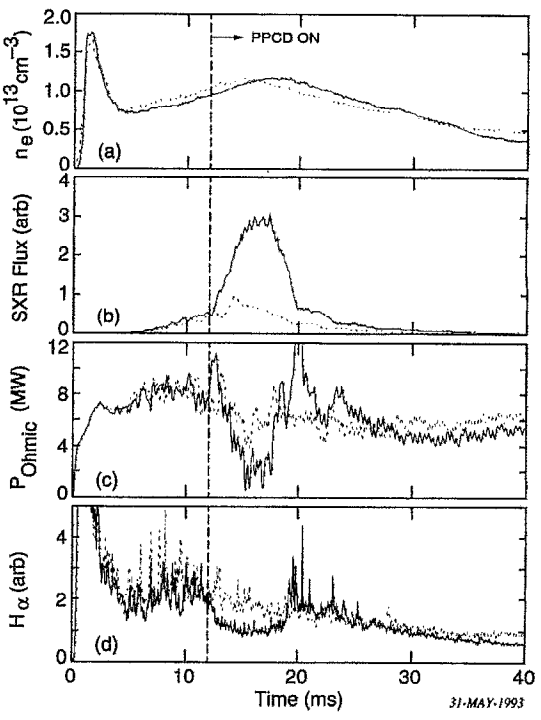

FIG. 5. Shot-averaged waveforms of (a) the central chord line-averaged electron density, (b) soft x-rays, (c) the Ohmic input power, and (d) H_α emission, with PPCD (solid curves) and without PPCD (dashed curves).

Assuming flat[17] temperature and parabolic density profiles (consistent with four interferometer chords inside $r/a=0.6$), the energy confinement time at $t=17$ ms is $\tau_E=3\pi^2a^2R\langle n_e\rangle(T_e+T_i)/P_{\text{Ohmic}}\approx 1.0$ ms without PPCD and $\tau_E\approx 2.2$ ms with PPCD. In standard RFP operation, τ_E scaling[16] in MST is weakly dependent on I_ϕ and n_e, varying little about $\tau_E=1$ ms. Because the stored magnetic energy changes during PPCD, the calculation of P_{Ohmic} was cross-checked using several equilibrium models.[11,12,18] The Polynomial Function Model[11] calculation, shown in Fig. 5(c), gives slightly larger values for P_{Ohmic} than the other models.

The particle confinement time τ_p also increases during PPCD. This is indicated by the 40% decrease in H_α emission and moderate rise in n_e. Particle transport modeling estimates τ_p increased by a factor of about 1.7 during PPCD.

PPCD reduces the anomalous plasma resistance. The change in toroidal plasma resistance from an increased poloidal field line twist during PPCD almost balances the change from reduced classical resistivity $\eta_{\text{sp}}\propto Z_{\text{eff}}/T_e^{3/2}$ (T_e increases, and Z_{eff} decreases). Therefore most of the reduction in P_{Ohmic} results from a 40% decrease in anomalous plasma resistance during PPCD. This conclusion is sensitive to the error in the T_e measurement, but a 50% T_e increase or

a dramatic T_e profile change is required to explain the P_{Ohmic} reduction classically. From the combined reductions in Z_{eff} and anomalous effects, the multiplier of the $Z=1$, flat temperature profile resistance decreases from 3 to 1.5. Typical of RFP plasmas, the ion temperature exceeds expectations for collisional heating by electrons. If the anomalous input power heats the ions, as is often assumed, then the reduced anomalous resistance and unchanged ion temperature during PPCD imply much reduced ion thermal loss.

Improved confinement during PPCD depends on the condition of the vacuum vessel wall. Clear improvement occurs with a boronized wall. (Solid target boronization is used in MST.[19]) Without boronization, enhanced impurity influx coincides with the PPCD pulse. Even with boronization, if the pulse is applied well after current peak, impurity-injection-free PPCD is difficult to obtain.

D. Comparison with stochastic diffusion model

A simplified analysis of the electron heat balance in the plasma core suggests that the improved confinement during PPCD results from reduced stochastic diffusion. Measurements of the magnetic-fluctuation-induced heat and particle fluxes in MST imply that the main loss in the core of the RFP results from particle convection in a stochastic magnetic field.[1,2] For this process, the radial electron heat flux is given by $Q_r^e=\frac{3}{2}T_e D_m v_{\text{th}}^{\text{ion}} \nabla n$ where $D_m \propto L_{\text{ac}}\tilde{B}_r^2$ is the magnetic diffusivity and L_{ac} is the magnetic fluctuation autocorrelation length. During PPCD, the confinement time doubled while the fluctuation amplitude decreased by ~25%. To see if these changes are consistent with the stochastic diffusion model, the electron heat balance is analyzed for a volume in the core of the plasma.

The dominant electron heat loss is assumed to be convective stochastic diffusion, while the input comes from classical Ohmic dissipation,

$$\int \eta_{\text{sp}} j_{\parallel}^2 \, dV = \int \tfrac{3}{2} T_e D_m v_{\text{th}}^{\text{ion}} \nabla n \, dS. \tag{2}$$

By restricting the heat balance to a volume in the core, radiation, and other losses can be neglected, and profile effects are minimized. The ions are hot, but they are not collisionally heated by the electrons. (The collisional ion heating power density is several percent of the central Ohmic dissipation $\eta_{\text{sp}} j_0^2$.)

Under these assumptions, the electron temperature dependence on other parameters is $T_e^{-5/2} \propto \tilde{B}_r^2 L_{\text{ac}} \sqrt{T_i} \nabla n / Z_{\text{eff}} j_0^2$, allowing a consistency check of the measured 25% increase in T_e, 25% reduction in $\tilde{B}$, a 20% reduction in Z_{eff}, and a (estimated) 20% increase in the central current density j_0 during the PPCD. The central density profile, the ion temperature T_i, and the $m=1$ spectral width (L_{ac}) did not change and should not affect T_e. The predicted increase in T_e from these parameter changes is ~30%, consistent with the measured increase. It appears that the core energy loss during PPCD is still dominantly stochastic diffusion.

Although reduced stochastic diffusion is encouraging, current profile control is hoped to free the plasma from magnetic-fluctuation-induced losses. This should occur when the magnetic fluctuation amplitude falls to a level where island overlap is avoided. To see how close the PPCD fluctuation amplitudes come to island overlap thresholds, the amplitudes of the core resonant $n=5-10$ $(m=1)$ modes are calculated for the case where the islands just overlap, as shown on the PPCD safety factor profile $q(r)$ in Fig. 6(a). The amplitudes $\tilde{b}_{rn}(r_s)$ are calculated from the island widths, $w=4\sqrt{L_s \tilde{b}_{rn}(r_s)/k_{\perp} B(r_s)}$, where r_s is the resonant surface radius and $L_s^{-1}=|r_s q'(r_s)/Rq^2(r_s)|$. Since radial profiles of the fluctuations are not measured, the profiles computed in the MHD code DEBS[15] are used to estimate the relationship between $\tilde{b}_{rn}(r_s)$ and the measurable amplitude $\tilde{b}_{\theta n}(a)$. The rule $\tilde{b}_{rn}(r_s) \approx 2.5 \tilde{b}_{\theta n}(a)$ is accurate in DEBS at Lundquist number $S=10^4$. (The experimental plasma has $S \sim 10^6$.)

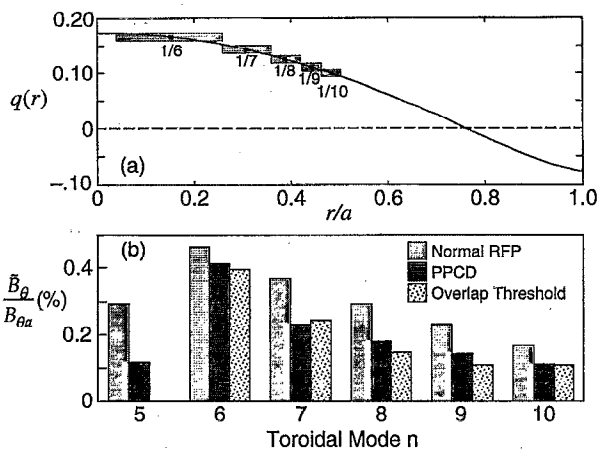

FIG. 6. (a) Safety factor profile estimated from equilibrium modeling at $t=17$ ms during PPCD. (b) The core-resonant fluctuation amplitudes $\tilde{b}_{\theta n}(a)$ in the standard RFP and during PPCD, in comparison with the estimated island overlap threshold amplitudes.

Figure 6(b) shows the measured $\tilde{b}_{\theta n}(a)$ fluctuation amplitudes for PPCD and normal RFP discharges (averaged over the sawtooth oscillation), in comparison with the predicted overlap threshold values. (During PPCD, $q_0<0.2$, so $m=1$, $n=5$ is nonresonant.) Not surprisingly, the fluctuation amplitudes in the normal RFP clearly exceed the island overlap threshold. During PPCD, the amplitudes fall to near threshold, but the islands probably still overlap in the core. Modest improvement in controlling the current profile and reducing the fluctuation amplitude may therefore dramatically improve confinement if island overlap can be avoided, and cross-field transport takes on a more classical behavior.

III. NONINDUCTIVE POLOIDAL CURRENT DRIVE

To sustain and enhance the improved confinement revealed by PPCD, electrostatic current injection, or RF current drive offer the possibility of steady-state current profile control in the RFP. Electrostatic current injection (helicity injection) employs electrically biased electrodes to drive current in the plasma. Spheromak[20] and similar configurations are traditionally formed this way, and the technique might provide a steady-state current drive solution for tokamaks.[21] RF current drive has a long history in tokamak research,

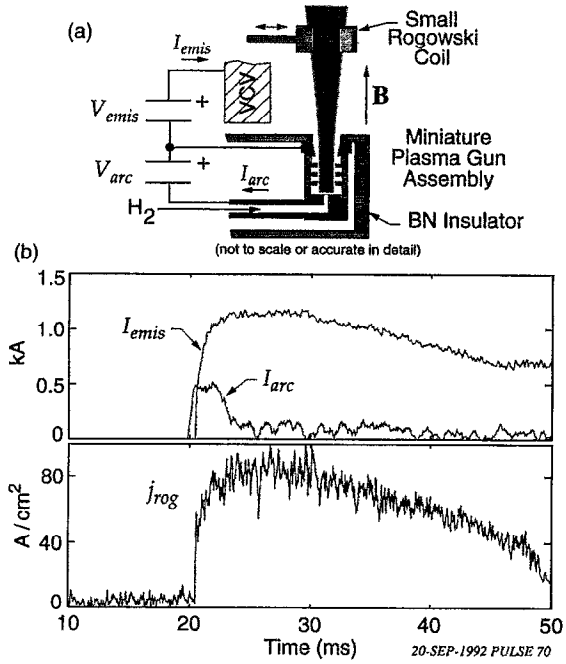

FIG. 7. (a) Schematic of a typical prototype plasma gun experiment in MST. (b) Typical waveforms of the arc current I_{arc}, emission current I_{emis}, and Rogowski current density j_{Rog}.

while its potential use in RFP plasmas is new research. This section briefly reviews these techniques with emphasis to MST applications.

A. Electrostatic current drive

The required features of the electrostatic current source include (i) high-current density ($\sim 2I_\phi/\pi a^2$), (ii) current emission in one direction along the magnetic field, and (iii) low impurity generation. A series of source prototype experiments on MST (including graphite and heated LaB_6 electrodes) led to an electrode design based on a small "plasma gun." The principal difficulties encountered with other sources are impurity generation, lack of unidirectional current emission, and arcing. The plasma gun[22] solves these problems by producing a high-density, cold, arc plasma encapsulated in a boron nitride insulator with a small hole through which current is extracted. The arc discharge is H_2 gas fed, to the metal impurities generated on the (molybdenum) arc electrodes are minimal.

A typical plasma gun experiment is shown schematically in Fig. 7(a). The gun assembly is inserted into the edge of the MST plasma, with the axis of the cylindrical arc channel oriented parallel to the equilibrium magnetic field. A small Rogowski coil separated from the plasma gun, but located on the same field line, detects the emitted current in the background plasma. In these prototype experiments, the gun plasma is biased negatively with respect to the vacuum vessel (VCV). In the full-scale experiment, anode electrodes may be required to control the plasma potential.

The arc, emission, and Rogowski currents are shown in Fig. 7(b). In this example, the bias voltages $V_{arc} \approx 50$ V and $V_{emis} \approx 250$ V were applied 20 ms after the background MST plasma was formed. The current density detected by the Rogowski coil was measured 60 cm from the gun. By scanning the Rogowski coil, virtually all of the emitted current is observed "attached" to the field line. When the gun is rotated 180°, no "backward" current density is detected by the Rogowski coil, indicating unidirectional current emission. (Even for weak current diffusion, the long connection length, and magnetic shear prevent detecting the "forward" emitted current when the gun is rotated 180°.).

MHD simulations[7,23] of electrostatic current injection indicate that the required auxiliary power to stabilize the core-resonant tearing fluctuations is about the same as the Ohmic input power from the inductive toroidal electric field. For $I_\phi = 400$ kA MST plasmas, $P_{Ohmic} \approx 6$ MW, and the projected total injected current requirement at $V_{emis} = 200$ V is ~30 kA. This is more than one gun can produce, so the full-scale experiment will utilize ~30 guns distributed on the plasma surface. This has the added feature of approximating toroidal symmetry found to be important in the MHD simulations.

B. Lower hybrid RF current drive

The distinguishing RFP features that affect RF current drive include a large ratio of the electron plasma frequency to cyclotron frequency ω_{pe}/ω_{ce} (ranging from 3 to 10), large magnetic shear, and a small trapped particle fraction. Theoretical investigations indicate that the fast wave[8] and lower hybrid (slow) wave[9] propagate in an RFP plasma, and should be useful for current drive. For the lower hybrid (LH) wave, the large ratio ω_{pe}/ω_{ce} necessitates a larger parallel refractive index $n_\parallel > 8$ for wave propagation than would be required in a comparable tokamak plasma. The propagating LH wave is predominantly electrostatic, and the wave vector **k** points almost perpendicular to the equilibrium magnetic field. The group velocity is almost perpendicular to **k**, so the wave energy and momentum propagate mostly in the poloidal direction, but with a small radially inward component, allowing access to the plasma.

To effect tearing stabilization, the LH wave must deposit its momentum at the correct radial location in the plasma. MHD simulations using the DEBS[15] code predict the target zone for the driven current is $r/a \approx 0.7$. To make this determination, an *ad hoc*, Gaussian-shaped, electron force was included in Ohm's law, and the location and amplitude of the force was adjusted to minimize the fluctuation amplitude.[9] The damping of the wave energy along a ray trajectory is estimated by calculating the imaginary part of the warm plasma dielectric tensor. For efficient electron Landau damping, $\omega/k_\parallel v_{the}$ should be 2–3 in the target zone. In a typical $I_\phi = 400$ kA MST plasma ($T_e \approx 200$ eV and $n \approx 8 \times 10^{18}$ m^{-3} at $r/a \approx 0.7$), a LH wave at $f = 250$ MHz with $n_\parallel = 10$ ($\lambda_\parallel = 12$ cm) completes about two poloidal turns before reaching the target zone. The analytic estimates for this typical MST plasma have been confirmed using a version of Brambilla's ray tracing code[24] modified to handle RFP equilibria. The code launches a single LH ray from the equatorial plane, and the ray integration proceeds until the energy falls to 0.1% of the initial value. Figure 8 shows the ray trajectory projected onto a poloidal plane and the driven current density profile.

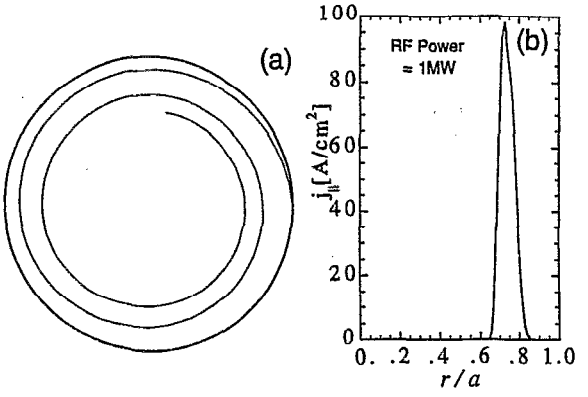

FIG. 8. (a) Poloidal plane projection of LH ray trajectory ($f=250$ MHz and $n_\parallel=10$). (b) Radial profile of RF-driven current density.

The efficiency of RF current drive is characterized locally by the quantity $\eta = j_\parallel^{rf}/p^{rf}$, which is theoretically calculable.[25] Often the global quantity I^{rf}/P^{rf} is reported, where I^{rf} and P^{rf} are the appropriately integrated current $j_\parallel^{rf}$ and power p^{rf} densities. For RFP profile control purposes, the *poloidal* RF-driven current I_θ^{rf} is important, and the estimated efficiency is $I_\theta^{rf}/P^{rf} \lesssim 0.5$ A/W for 400 kA MST plasmas. (Since $I_\theta \approx 5 I_\phi$, this corresponds to $I_\phi^{rf}/P^{rf} \lesssim 0.1$ A/W for toroidal current drive in a tokamak with equivalent parameters.) The estimated deposited power requirement is $P^{rf} \gtrsim 1$ MW for tearing stabilization in MST.

IV. SUMMARY

In summary, inductive poloidal current drive flattens the current density profile, slows the growth of $m=1$ tearing fluctuations, suppresses their associated sawteeth, and doubles the energy and particle confinement times. A reduction in anomalous plasma resistance suggests PPCD reduces the dynamo effect. The improved plasma state exhibits small sawtooth-like events, but they are preceded by $m=0, n\sim 1$ instability, rather than $m=1, n\sim 6$ instability.

Although PPCD does not eliminate tearing fluctuation, clear correlation exists between improved confinement, current profile flattening, and modest fluctuation suppression. A simplified heat balance in the plasma core suggests the dominant heat loss mechanism during PPCD is still stochastic diffusion, but an analysis of the magnetic island structure indicates the core-resonant fluctuation amplitudes during PPCD approach island overlap threshold values. Modest improvement in controlling the current profile and reducing the fluctuation amplitude may therefore dramatically improve confinement if island overlap can be avoided and cross-field transport takes on a more classical behavior.

To sustain and enhance an improved confinement state, electrostatic and RF current drive are being developed for the RFP. In MST, prototype experiments led to an electrostatic current injector based upon a small plasma gun. Large, unidirectional current is obtained without significant impurity generation. Tearing stabilization will be attempted in MST by replicating this injector to meet the MHD predicted ~30 kA and ~6 MW injection requirements.

The lower hybrid wave is a promising candidate for efficient poloidal current drive in the RFP. Accessibility, energy absorption, and current drive have been evaluated through a combination of analytical and computational ray tracing. Experimental plans on MST include low-power RF tests to confirm wave propagation, but a full power test of tearing stabilization is a longer term goal.

ACKNOWLEDGMENTS

The authors are grateful for the assistance of J. Frank, D. Holly, J. Laufenberg, T. Lovell, K. Mirus, M. Stoneking, and M. Thomas. We also acknowledge P. Figgliozi for computational assistance.

This work was supported by the U. S. Department of Energy Grant No. DE-FG02-85ER53212 and Contract No. DE-AC03-89ER51114.

[1] G. Fiksel, S. C. Prager, W. Shen, and M. Stoneking, Phys. Rev. Lett. **72**, 1028 (1994).
[2] M. R. Stoneking, S. A. Hokin, S. C. Prager, G. Fiksel, H. Ji, and D. Den Hartog, Phys. Rev. Lett. **73**, 549 (1994).
[3] R. N. Dexter, D. W. Kerst, T. H. Lovell, S. C. Prager, and J. C. Sprott, Fusion Technol. **19**, 131 (1991).
[4] For example, I. H. Hutchinson M. Malacarne, P. Noonan, and D. Brotherton-Ratcliffe, Nucl. Fusion **24**, 59 (1984); K. Hattori, Y. Hirano, T. Shimada, Y. Yagi, Y. Maejima, I. Hirota, and K. Ogawa, Phys. Fluids B **3**, 3111 (1991); H. Ji, H. Toyama, K. Miyamoto, S. Shinohara, and A. Fujisawa, Phys. Rev. Lett. **67**, 62 (1991).
[5] J. D. Callen, Phys. Rev. Lett. **39**, 1540 (1977); A. B. Rechester and M. N. Rosenbluth, Phys. Rev. Lett. **40**, 38 (1978).
[6] For example, V. Antoni and S. Ortolani, Plasma Phys. **25**, 799 (1983); D. Brotherton-Ratcliffe, C. G. Gimblett, and I. H. Hutchinson, Plasma Phys. Controlled Fusion **24**, 59 (1984); R. J. La Haye, T. N. Carlstrom, R. R. Goforth, G. L. Jackson, M. J. Schaffer, T. Tamano, and P. L. Taylor, Phys. Fluids **27**, 2576 (1984); A. Almagri, S. Assadi, S. C. Prager, J. S. Sarff, and D. W. Kerst, Phys. Fluids B **4**, 4080 (1992); P. R. Brunsell, Y. Yagi, Y. Hirano, Y. Maejima, and T. Shimada, Phys. Fluids **5**, 885 (1993).
[7] Y. L. Ho, Nucl. Fusion **31**, 341 (1991).
[8] S. Shiina, K. Saito, Y. Kondoh, H. Ishii, T. Shimada, and Y. Hirano, in *Proceedings of the 19th EPS Conference on Controlled Fusion and Plasma Physics*, Innsbruck, 1992 (European Physical Society, Petit-Lancy, Switzerland, 1992), Vol. 16C, p. 917; H. Ishii, Y. Kondoh, T. Shimada, Y. Hirano, S. Shiina, and K. Saito, in *Proceedings of the 20th EPS Conference on Controlled Fusion and Plasma Physics*, Lisbon, 1993 (European Physical Society, Petit-Lancy, Switzerland, 1993), Vol. 17C, p. 495.
[9] E. Uchimoto, M. Cekic, R. W. Harvey, C. Litwin, S. C. Prager, J. S. Sarff, and C. R. Sovinec, Phys. Plasmas **1**, 3517 (1994).
[10] J. S. Sarff, S. A. Hokin, H. Ji, S. C. Prager, and C. R. Sovinec, Phys. Rev. Lett. **72**, 3670 (1994).
[11] J. C. Sprott, Phys. Fluids **31**, 2266 (1988).
[12] V. Antoni, D. Merlin, S. Ortolani, and R. Paccagnella, Nucl. Fusion **26**, 1711 (1986).
[13] R. G. Watt and R. A. Nebel, Phys. Fluids **26**, 1168 (1983); S. Hokin, A. Almagri, S. Assadi, J. Beckstead, G. Chartas, N. Crocker, M. Cudzinovic, D. Den Hartog, R. Dexter, D. Holly, S. Prager, T. Rempel, J. Sarff, E. Scime, W. Shen, C. Spragins, C. Sprott, G. Starr, M. Stoneking, and C. Watts, Phys. Fluids B **3**, 2241 (1991).
[14] In a cylinder, $\tilde{b}_{\theta 0n}$ vanishes, but toroidal effects allow finite $\tilde{b}_{\theta 0n}$ for "$m=0$" instability.
[15] D. D. Schnack, D. C. Barnes, Z. Mikic, D. S. Harned, and E. J. Caramana, J. Comput. Phys. **70**, 330 (1987).
[16] S. Hokin, A. Almagri, M. Cekic, B. Chapman, N. Crocker, D. J. Den Hartog, G. Fiksel, J. Henry, D. Holly, H. Ji, S. Prager, J. Sarff, W. Shen, M. Stoneking, and C. Watts, in Ref. 8, Vol. II, p. 475.
[17] This assumption is motivated by the stochastic nature of the confining magnetic field. Limited measurements in standard MST RFP discharges are consistent with a flat T_e profile.
[18] K. F. Schoenberg, R. F. Gribble, and J. A. Phillips, Nucl. Fusion **22**, 1433 (1982).

[19]D. J. Den Hartog, M. Cekic, G. Fiksel, S. Hokin, R. Kendrick, S. Prager, and M. Stoneking, J. Nucl. Mat. **200**, 177 (1993).
[20]T. Jarboe, Fusion Technol. **15**, 7 (1989).
[21]M. Ono, G. J. Greene, D. Darrow, C. Forest, H. Park, and T. H. Stix, Phys. Rev. Lett. **59**, 2165 (1987); B. A. Nelson, T. R. Jarboe, D. J. Orvis, L. A. McCullough, J. Xie, C. Zhang, and L. Zhou, Phys. Rev. Lett. **72**, 3666 (1994).
[22]G. I. Dimov, G. V. Roslyakov, and V. Ya. Savkin, Sov. Prib. Tech. Exp. **20**, 29 (1977); G. Fiksel, M. Kishinevsky, and N. Hershkowitz, Phys. Fluids B **3**, 834 (1991).
[23]C. R. Sovinec, S. C. Prager, and Y. L. Ho, Bull. Am. Phys. Soc. **37**, 1608 (1992).
[24]M. Brambilla, Comput. Phys. Rev. **4**, 71 (1986).
[25]D. A. Ehst and C. F. F. Karney, Nucl. Fusion **31**, 1933 (1991).